ORGANIC CHEMISTRY FRONTIERS

RESEARCH ARTICLE

View Article Online
View Journal



Cite this: DOI: 10.1039/d5qo00981b

# 1,6-Hydrosulfonylation of *p*-quinone methides enabled *via* strain-release-/aromaticity-driven alkyl radical generation and $SO_2$-capture: synthesis and antiproliferative studies of sulfonylated diarylmethanes

Dipun Kumar Penthi, [a] Tonish Kumar Sahu, [a] Rahimuddin Khan, [a] Shanti Gopal Patra [b] and Tabrez Khan *[a]

The integration of γ-keto sulfones, despite being medicinally relevant building blocks, with the bioactive diarylmethane motif remains elusive. On the other hand, the fixation of $SO_2$ into organic molecules for accessing value-added products is gaining wide attention in organic synthesis. Herein, we disclose the 1,6-hydrosulfonylation of *p*-quinone methides *via* the strain-release driven ring-scission of strained 3°-cyclopropanols in the presence of a $SO_2$-surrogate like $K_2S_2O_5$ and a Brønsted acid under visible-light photoredox catalysis to access a library of γ-keto alkylsulfonylated diarylmethanes in moderate to good yields. Also, the 1,6-hydrosulfonylation of *p*-quinone methides has been developed *via* aromaticity-driven bond-scission in pro-aromatics like 4-alkyl-1,4-DHPs in the presence of $K_2S_2O_5$ and a Brønsted acid under visible-light photoredox catalysis to access a library of alkylsulfonylated diarylmethanes. The efficiency of the developed reactions has been established through broad substrate-scope studies, and the mechanistic probing studies have been complemented with DFT calculations to support the proposed mechanisms. In addition, antiproliferative studies revealed oral cancer activity for some of the synthesized sulfonylated diarylmethane derivatives.

Received 3rd July 2025,
Accepted 6th September 2025

DOI: 10.1039/d5qo00981b

rsc.li/frontiers-organic



## Introduction

The unsymmetrical diarylmethane (DAM) motif is quite ubiquitous in the cyclolignan and secolignan subclasses of lignans,[1,2] among other classes of natural products, as exemplified by podophyllotoxin[3] and peperomin H[4] respectively. Besides, cetirizine[5] represents a synthetic molecule of pharmaceutical origin (Fig. 1A), underscoring the significance of the DAM motif as a privileged scaffold.[6] Interestingly, the merger of the DAM motif with sulfones has proven to be quite rewarding in synthetic organic chemistry and from a medicinal chemistry perspective, in terms of reaping better therapeutic potential. The resultant diarylmethyl sulfones (DAMS) have emerged as superior pharmacophoric motifs displaying a wide range of activities in diverse pharmaceutical applications (Fig. 1B).[7] In this direction, to further amplify the scope of DAMS, we were motivated to integrate the DAM motif with γ-keto sulfones and test the efficacy of the resultant DAMS synthetically and therapeutically. Our motivation was backed by the reputation of γ-keto sulfones as medicinally relevant building blocks by featuring in commercially relevant agrochemicals[8] and pharmaceuticals.[9,10] Also, the footprint of these fragments in functional materials,[11,12] in addition to their inherent versatility as useful synthetic intermediates,[13–16] made them a lucrative choice. Additionally, to the best of our knowledge, there is no literature precedent for synthesizing γ-keto sulfonylated DAMs, while synthetic routes towards sulfonylated DAMs are documented sporadically.

Besides transition-metal catalyzed cross-coupling reactions,[17–19] synthetic access to DAMS has been traditionally demonstrated *via* $2e^-$ retrosynthetic disconnections typically involving the 1,6-conjugate addition of arylsulfinyl anions generated from arylsulfonylhydrazides,[7,20] arylsulfinic acid sodium salts,[21] or tosylmethyl isocyanide[22,23] onto *para*-quinone methides (*p*-QMs). Also, the radical-based *p*-QM bis-functionalization strategy[24] involving oxidant-assisted generation of aryl sulfonyl radicals from arylsulfonylhydrazides has recently been reported (Fig. 1C). In contrast, there are hardly

[a]*Organic Synthesis Laboratory, Department of Chemistry, School of Basic Sciences, Indian Institute of Technology Bhubaneswar, Argul-752050, Odisha, India. E-mail: tabrez@iitbbs.ac.in; Tel: +91-67-4713-5614*
[b]*Department of Chemistry, National Institute of Technology Silchar, Silchar-788010, India*

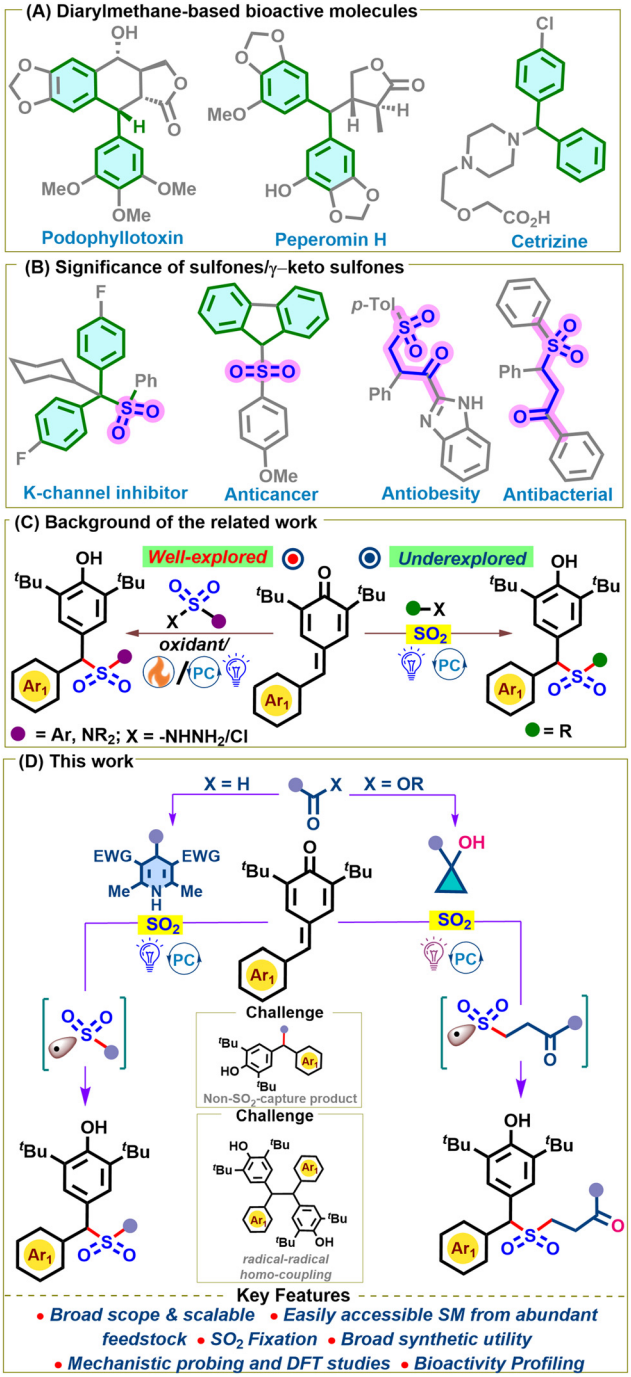


**Fig. 1** Representative examples of (A) DAM-based bioactive compounds; (B) potent compounds containing sulfone-/γ-keto sulfone building blocks; (C) previous work; and (D) present strategy.

any visible-light photoredox-catalyzed radical logic-based strategies directed towards accessing DAMS, let alone those involving $SO_2$-capture. The recent report by Mei *et al.* for accessing diarylmethyl sulfonamides employing sulfamoyl chloride[25] and *p*-QMs under photoredox catalysis constitutes one such report. In contrast, the one by Wu and coworkers on synthesizing DAMS utilizing alkyltrifluoroborate salts and *p*-QMs is the sole report involving $SO_2$-capture *via* photoredox catalysis.[26]

$SO_2$ is one of the serious concerns among other global anthropogenic emissions.[27] Due to the enormous $SO_2$ production every year, the fixation of $SO_2$ into small molecules has gained a reputation in organic synthesis.[28–30] In particular, accessibility to easy-to-handle organic surrogates like DABCO·$(SO_2)_2$ or DABSO and rongalite, among a few others, along with bisulfites/metabisulfites of sodium/potassium as inorganic surrogates, has fueled further interest in $SO_2$-fixation into organic molecules.[31–36] On the other hand, the operational simplicity and easy reaction setup customization, besides mild reaction conditions, have made visible-light photocatalysis the preferred choice in industry and academia for leveraging unique reactivities to develop novel synthetic transformations.[37–43]

Indeed, our ongoing interest[44–46] in utilizing anthropogenic gases like $SO_2$ and its surrogates for value-added chemical synthesis through sustainable means has led us to choreograph the visible-light photoredox catalyzed 1,6-hydrosulfonylation of *p*-QMs involving $SO_2$-fixation *en route* to γ-keto sulfonylated unsymmetrical diarylmethanes for the first time, as well as sulfonylated unsymmetrical diarylmethanes from readily accessible feedstock chemicals (Fig. 1D). In this direction, our working hypothesis was to facilitate the 1,6-hydrosulfonylation of *p*-QMs with the aid of (a) the γ-keto alkyl sulfonyl radical and (b) the alkyl sulfonyl radical. In turn, access to the γ-keto sulfonyl radical was strategized *via* strain-release-driven β-keto alkyl radical generation from small-ring carbocycles such as cyclopropanols. Cyclopropanols, by virtue of their innate ring strain,[47–53] under photoredox catalysis, *via* either an oxidative single electron transfer (SET) process or a hydrogen-atom transfer (HAT) process, were postulated to undergo β-scission and subsequent $SO_2$-capture to furnish the γ-keto sulfonyl radical for the planned 1,6-bisfunctionalization of *p*-QMs (Fig. 1D).In contrast, the easy accessibility and favorable redox properties of pro-aromatics like 4-alkyl-1,4-dihydropyridines[54] (DHPs) motivated us to access the alkyl sulfonyl radical through aromaticity-driven alkyl radical generation from 4-alkyl-1,4-DHPs and ensuing $SO_2$-capture, for the envisioned bisfunctionalization under photoredox catalysis (Fig. 1D). At the same time, we also anticipated some challenges in the successful realization of each of these hypotheses, such as (i) the radical–radical homo-coupling reaction of the generated diarylmethane radical, (ii) the radical–radical cross-coupling reaction between the generated diarylmethane radical and the β-keto alkyl radical without $SO_2$-capture, leading to a non-sulfonylated cross-coupled product, and (iii) the undesired radical–radical cross-coupling reaction of the generated species, affording HAT-/other recombination products. Despite these challenges, we succeed in disclosing herein a visible-light photoredox catalyzed bisfunctionalization strategy to access γ-keto sulfonylated/alkyl sulfonylated DAMs *via* strain-release-driven/aromaticity-driven radical generation and $SO_2$-fixation. A broad substrate scope has been demonstrated with respect to each of the reactants employed for the two strategies to establish a library of DAMS. Furthermore, an array of useful

post-synthetic modifications has been demonstrated utilizing the available functional group handle in the accessed scaffold.

## Results and discussion

To test our hypothesis, we commenced our initial investigation employing *p*-QM **1a** and 1-phenylcyclopropanol **2a** as the model substrates. An intensive optimization study involving screening different photoredox catalysts (PCs) and light sources, besides testing other variables, including the $SO_2$ source, oxidant, and solvent, led us to the optimized conditions, as depicted in Fig. 2. Irradiation of an acetonitrile solution of **1a** (1 equiv.) and **2a** (2 equiv.) with a purple LED ($\lambda_{max}$ = 390 nm) in the presence of TFA (1 equiv.), $K_2S_2O_5$ (1.5 equiv.) and Eosin Y (2 mol%) at room temperature for 1.5 h furnished the desired γ-keto alkylsulfonylated DAM **3aa** with an isolated yield of 90% (Fig. 2A, column 1). Encouraged by this outcome, the next step was to investigate the effect of light sources on the reaction. Replacing the purple LED ($\lambda_{max}$ = 390 nm) in the reaction with a blue LED ($\lambda_{max}$ = 456 nm)/green LED ($\lambda_{max}$ = 525 nm) resulted in an inferior yield of the product (Fig. 2A, columns 14 and 15). Although marginal product formation was observed in the individual absence of either light, PC, or acid, no product formation was observed in the combined absence of light, PC, and acid (Fig. 2A, columns 9–12), highlighting their essentiality for the reaction. Additionally, on replacement of Eosin Y with other investigated PC-2 to PC-6, the desired product formation was observed, albeit in lower yields (Fig. 2A, columns 2–6). This indeed proved **PC-1** to be an ideal PC compared to the other investigated ones to facilitate strain-release-driven cyclopropanol ring opening. Similarly, replacement of $K_2S_2O_5$ with other $SO_2$ surrogates, such as $Na_2S_2O_5$, $NaHSO_3$, and DABSO, did not help improve the yield of the desired product **3aa** (Fig. 2A, columns 7–9). Lastly, the solvent screening studies revealed DCM/DCE to offer almost the same results, while using other solvents resulted in the diminution of the isolated yield of **3aa** [(Fig. 2A, columns 16–19), refer to the SI for further details about optimization studies].

Similarly, for the reaction between **1a** and **4a**, an intensive optimization endeavor involving screening different PCs and light sources and testing other variables led us to the optimized conditions, as depicted in Fig. 2. The optimal efficiency of the photocatalyzed process was found with the blue-LED irradiation (456 nm) of a DCE solution of **1a** (1.0 equiv.) and **4a** (2.5 equiv.) under an inert atmosphere at room temperature for 2 h in the presence of TFA (1.5 equiv.), $K_2S_2O_5$ (2 equiv.), $K_2S_2O_8$ (1.5 equiv.) and $AgNO_3$ (20 mol%) while employing Eosin Y (5 mol%) as the PC to access **5aa** in 75% yield (Fig. 2B, column 1). The complete suppression of the reaction in the absence of light and a profound decrease in reaction efficiency

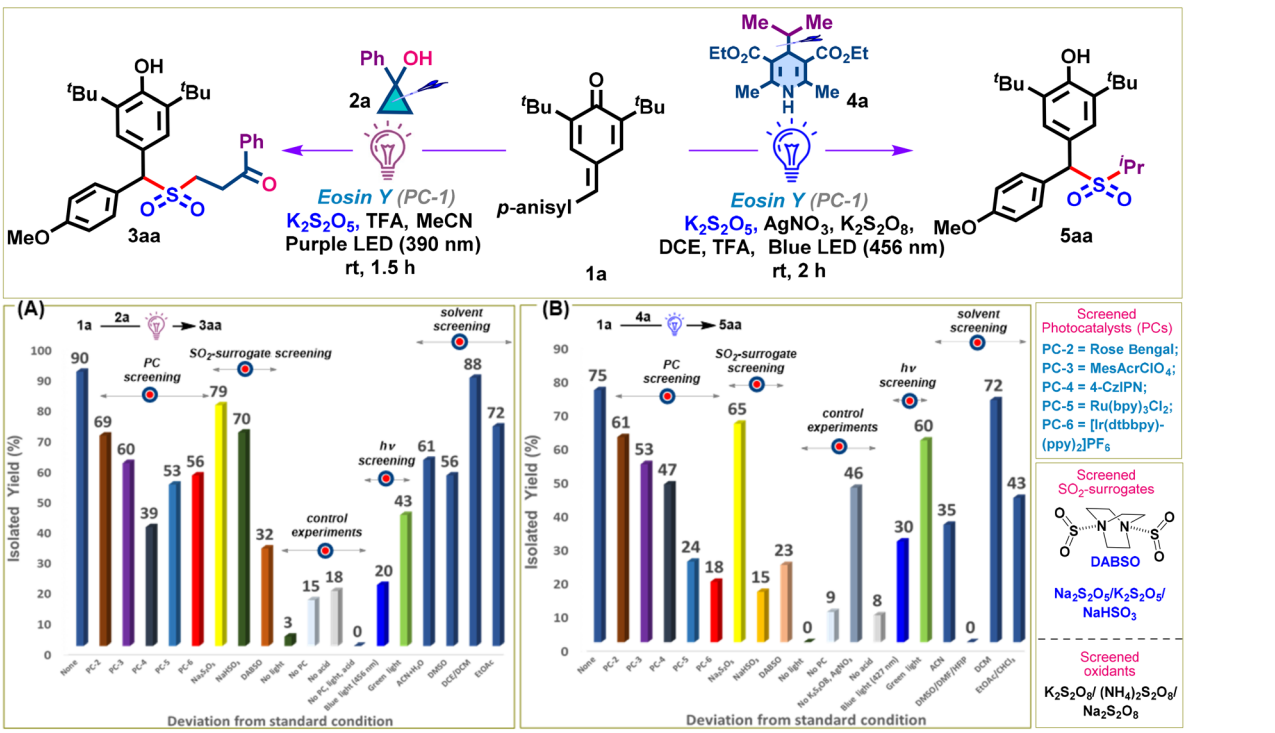


**Fig. 2** Reaction optimization. (A) Reaction conditions: **1a** (0.12 mmol, 1 equiv.), **2a** (0.24 mmol, 2 equiv.), TFA (0.12 mmol, 1 equiv.), $K_2S_2O_5$ (0.18 mmol, 1.5 equiv.), and Eosin Y (2 mol%) in MeCN (2 mL) irradiated with Kessil purple LED light (390 nm) at rt in a $N_2$ atmosphere for 1.5 h. (B) Reaction conditions: **1a** (0.12 mmol, 1 equiv.), **4a** (0.30 mmol, 2.5 equiv.), TFA (0.18 mmol, 1.5 equiv.), $K_2S_2O_5$ (0.24 mmol, 2 equiv.), $K_2S_2O_8$ (0.18 mmol, 1.5 equiv.), $AgNO_3$ (20 mol%), and Eosin Y (5 mol%) in DCE (2 mL) irradiated with Kessil blue LED light (456 nm) at rt in a $N_2$ atmosphere for 2 h.

in the absence of **PC-1** and acid confirmed the essentiality of both components for the reaction (Fig. 2B, columns 10, 11 and 13). Inferior yields of **5aa** were obtained in either of the following cases: when **PC-1** was substituted with other investigated catalysts (Fig. 2B, columns 2–6) or when the 456 nm blue-LED was substituted with other light sources (Fig. 2B, columns 14 and 15). Similarly, replacing $K_2S_2O_5$ with other investigated $SO_2$-surrogates affected the yield of **5aa** to varying extents (Fig. 2B, columns 7–9). Control experiments demonstrated that $K_2S_2O_8$ and $AgNO_3$ play a crucial role in synergistically assisting **PC-1** in improving the yield of **5aa**, as their absence resulted in a substantial decrease in the yield (Fig. 2B, column 12). Solvent screening studies indicated DCE/DCM to be the ideal one among the other investigated solvents for this transformation [(Fig. 2B, columns 16–19), refer to the SI for further details about optimization studies].

With the optimized conditions in hand, the stage was set to demonstrate the robustness of the developed strategies through broad substrate-scope studies to unleash the multiple diversity creation junctures for the accessed DAMS **3** and **5**. To begin with, the scope and generality of *p*-QMs and cyclopropanols for the photoredox-catalyzed reaction were tested first (Scheme 1a). The reaction of *p*-QM **1b**, as well as the analogs **1c–1i** bearing either electron-donating ($C_4$-OH, OAc) or electron-withdrawing (–F, –Cl, –Br, –CN, and $–NO_2$) substituents at the *para*-position of the aryl ring in *p*-QMs, with **2a** afforded the desired products **3ba–ia** in moderate to good yields (73–86%). Also, the influence of both types of substituents on the *ortho*- and *meta*-positions of the aryl ring in *p*-QM was tested. It must be noted that these substituents were found to have minimal effects on the reactivity, as DAMS **3ja–qa** were smoothly accessed and offered the realm of post-synthetic modification. Then, chemoselective 1,6-hydrosulfonylation in *p*-QM **1r**, with an O-allyl arm, was demonstrated smoothly. The analogs with a disubstituted aryl residue in *p*-QMs were also tested under the optimized conditions to access **3qa–va**. Notably, the scope was also extended to include 2-thiophenyl- and 2-pyridyl-tethered *p*-QMs to access **3wa** and **3xa**, respectively, in moderate yields. However, attempts to access the DAMS **3ya** and **3za** from *p*-QMs tethered with 9-anthracenyl and 4-pyridinyl units were unsuccessful. Lastly, we also extended the scope of the developed conditions to the 1,4-hydrosulfonylation of *in situ* generated *o*-QM (**1′a**) to access **3′aa** effortlessly.

Next, attention was directed toward exploring the scope of various cyclopropanols for hydrosulfonylation of *p*-QM **1a**, and the results are summarized in Scheme 1b. After thoroughly testing 1-phenylcyclopropanol in coupling with diverse *p*-QMs, the tolerance of other 1-phenylcyclopropanol derivatives bearing electron-donating substituents (–Me, –OMe, and –Ph) as well as electron-withdrawing substituents (–F, –Cl, and –Br) at either the *ortho* or the *para* position of the aryl ring was demonstrated by accessing DAMS (**3ab–3af**) in moderate to good yields (60–81%). Also, cyclopropanols with disubstituted aryl rings were tolerated, as **3ag** and **3ah** were accessed easily. Furthermore, we could demonstrate the feasibility of the reaction employing diverse alkyl-substituted cyclopropanols. For instance, linear long 1°-alkyl chain substituted, cyclohexyl substituted, and 1-adamantyl substituted cyclopropanols **2i–k** were employed to access **3ai–3ak**, respectively, in 42–75% yields. Also, cyclopropanols with unsubstituted and substituted benzyl groups showcased good reactivity, as DAMS **3al** and **3am** were obtained in good yields. Eventually, the efficacy of the developed protocol for pharmaceutically relevant molecules was demonstrated by accessing **3an–3ap** in satisfactory yields, through the photoredox catalyzed reaction of **1a** with ibuprofen-, naproxen-, and gemfibrozil-derived cyclopropanols while ensuring $SO_2$ fixation.

After establishing a library of γ-keto sulfonylated DAMs **3** through substrate scope investigation of **1** and **2**, the next task of demonstrating hydroalkylsulfonylation employing diverse *p*-QMs **1** and 4-alkyl-1,4-DHP **4a**, as the C-centered radical source, in the presence of $SO_2$ gas was taken in hand (Scheme 2a). The reaction of *p*-QM 1b, as well as the analogs **1c–1i** bearing either electron-donating ($C_4$-OH, OAc) or electron-withdrawing (–F, –Cl, –Br, –CN, and $–NO_2$) substituents at the *para*-position of the aryl ring in *p*-QMs, with **4a** afforded the desired products **5ba–ia** in moderate to good yields (68–77%). Also, *p*-QMs with aryl rings with *ortho*- and *meta*-substituted electron-donating/withdrawing groups were tested, and the corresponding DAMS **5ja–ra** were accessed smoothly. Also, the analogs with the disubstituted aryl residue in *p*-QMs were tested under the optimized conditions to access **5sa-va**. Gratifyingly, we could confirm the structure of **5sa** (CCDC 2441977) through X-ray crystallographic studies.[55] Notably, the scope was also extended to include 2-thiophenyl- and 2-pyridyl-tethered *p*-QMs to access **5wa** and **5xa**, respectively, in moderate yields. However, attempts to access the DAMS **5ya** and **5za** from *p*-QMs tethered with 9-anthracenyl and 4-pyridinyl units were unsuccessful. Lastly, we also extended the scope of the developed conditions to the 1,4-hydrosulfonylation of *in situ* generated *o*-QM (**1′a**) to access **5′aa** effortlessly.

Thereafter, we redirected our focus to exploit a plethora of diversely substituted 4-alkyl-DHPs for reaction with *p*-QM **1a**. As shown in Scheme 2b, C-centered radicals produced from diverse 4-(2°-alkyl)-1,4-DHPs were successfully transferred while fixing $SO_2$ to afford DAMS in moderate to good yields (**5ab–ad**). Acyclic and cyclic 2°-alkyl-substituted DHPs with distal functionalities displayed better reactivity under optimized reaction conditions, affording the desired products (**5ae–ag**). A DHP bearing a tetrahydrofuran ring was also found to be compliant, delivering the corresponding product **5ah** in 72% as an inseparable 1 : 1 diastereomeric mixture. Also, we could succeed in accessing **5ai–al** while using the 3°-alkyl and homobenzylic groups derived from DHPs **4i–l** in $SO_2$ fixation.

Next, we shifted our attention towards highlighting the scalability and synthetic utility of the accessed DAMS through some useful downstream functional transformations shown in Scheme 3. The photoredox-catalyzed couplings of **1a** with **2a** and **4a**, respectively, at a 3 mmol scale under the established conditions afforded the corresponding DAMS **3aa** and **5aa** in

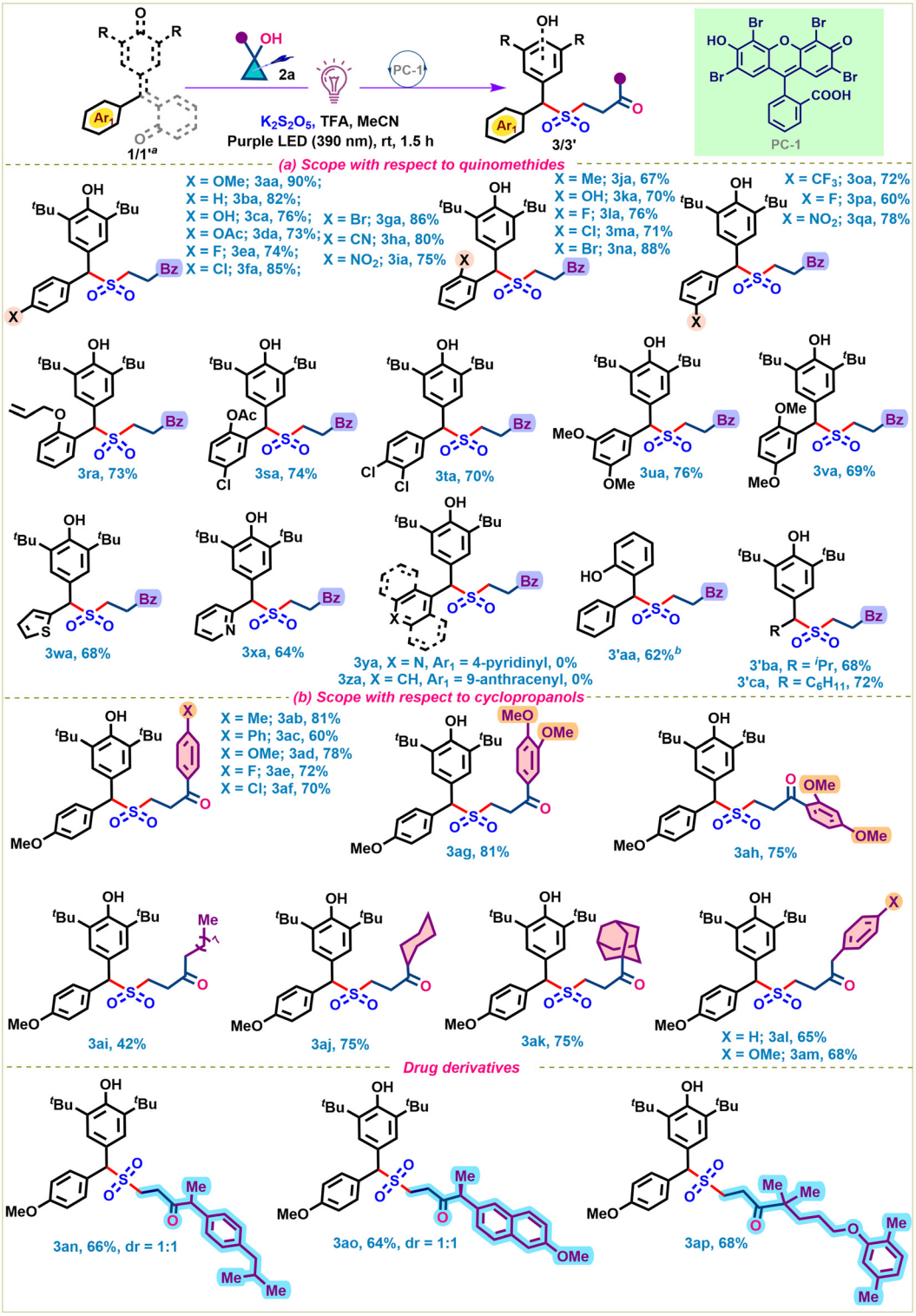


**Scheme 1** Substrate scope for 1,6/1,4-hydrosulfonylation of QM **1** using **2**. [a] **1'** was generated *in situ* from 2-(hydroxy(phenyl)methyl)phenol; [b] $BF_3{\cdot}OEt_2$ was used instead of TFA.

74% and 65% yields, respectively. Then, carefully crafted DDQ-mediated oxidation was demonstrated on both **3aa** and **5aa** to access sulfonylated *p*-QMs **6 and 7**, respectively. Also, access to the γ-oxime alkylsulfonylated DAM **8** was demonstrated from **3aa** effortlessly. Then, **3aa** was utilized to demonstrate the chemoselective reductive deoxygenation of the sulfone to sulfide **9**. Esterification of the phenolic-OH in **3ca** was demonstrated, besides the desulfonylative oxidation of **3aa**/**5aa** to

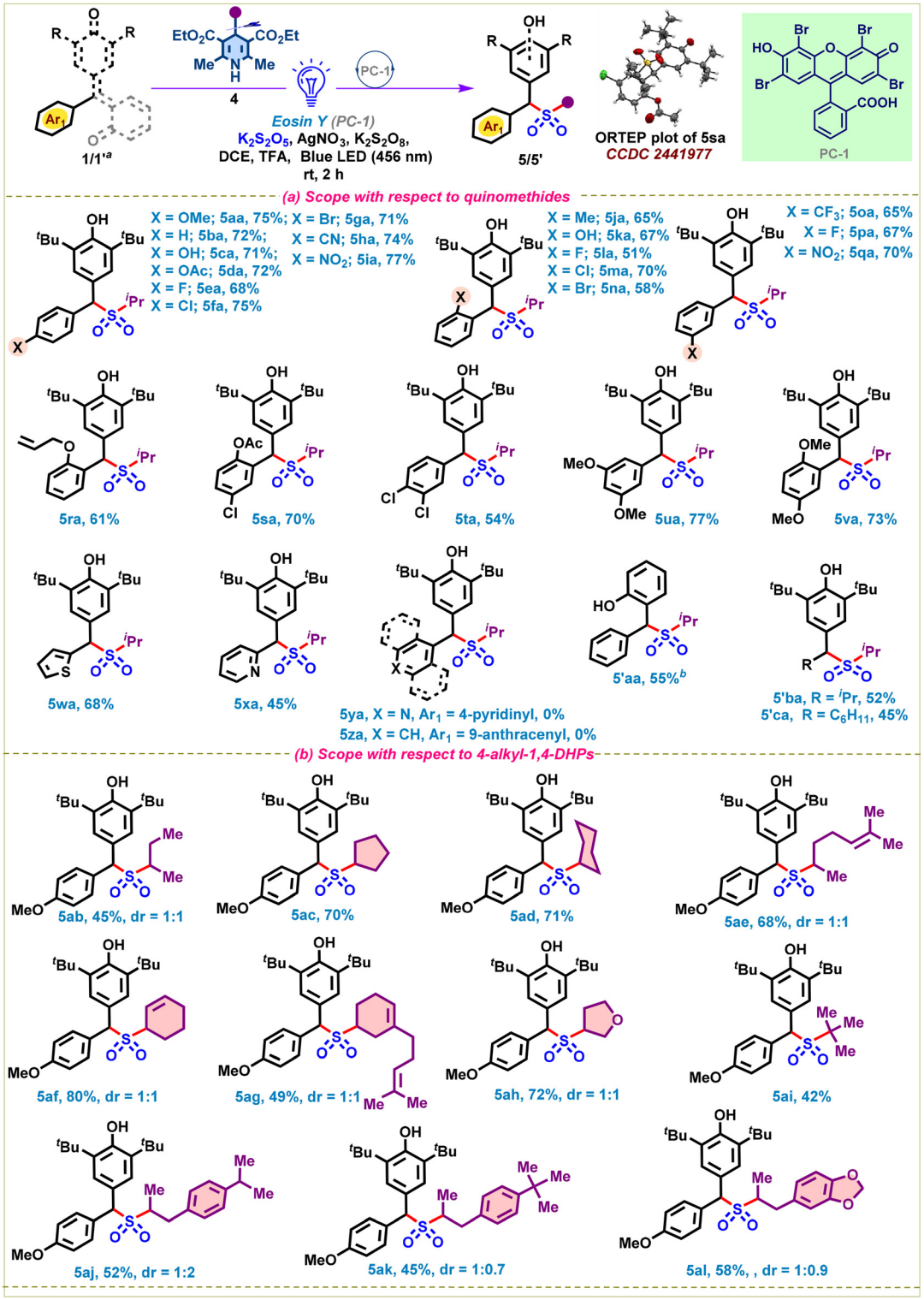


**Scheme 2** Substrate scope for 1,6/1,4-hydrosulfonylation of QM **1** using **4**. [a] **1'** was generated *in situ* from 2-(hydroxy(phenyl)methyl)phenol; [b] $BF_3{\cdot}OEt_2$ was used instead of TFA.

benzophenone **11**. Furthermore, a Ru-catalyzed cross-metathesis reaction was demonstrated on **5ra** to access the α,β-unsaturated ester **12**. Lastly, we could demonstrate desulfonylative C–N bond formation *via* benzotriazole addition on **3aa**/**5aa** to access diarylmethane-substituted benzotriazoles **13** and **14**, respectively.

We next ventured to gain insights into the underlying mechanisms for the reactions involving the coupling of *p*-QMs

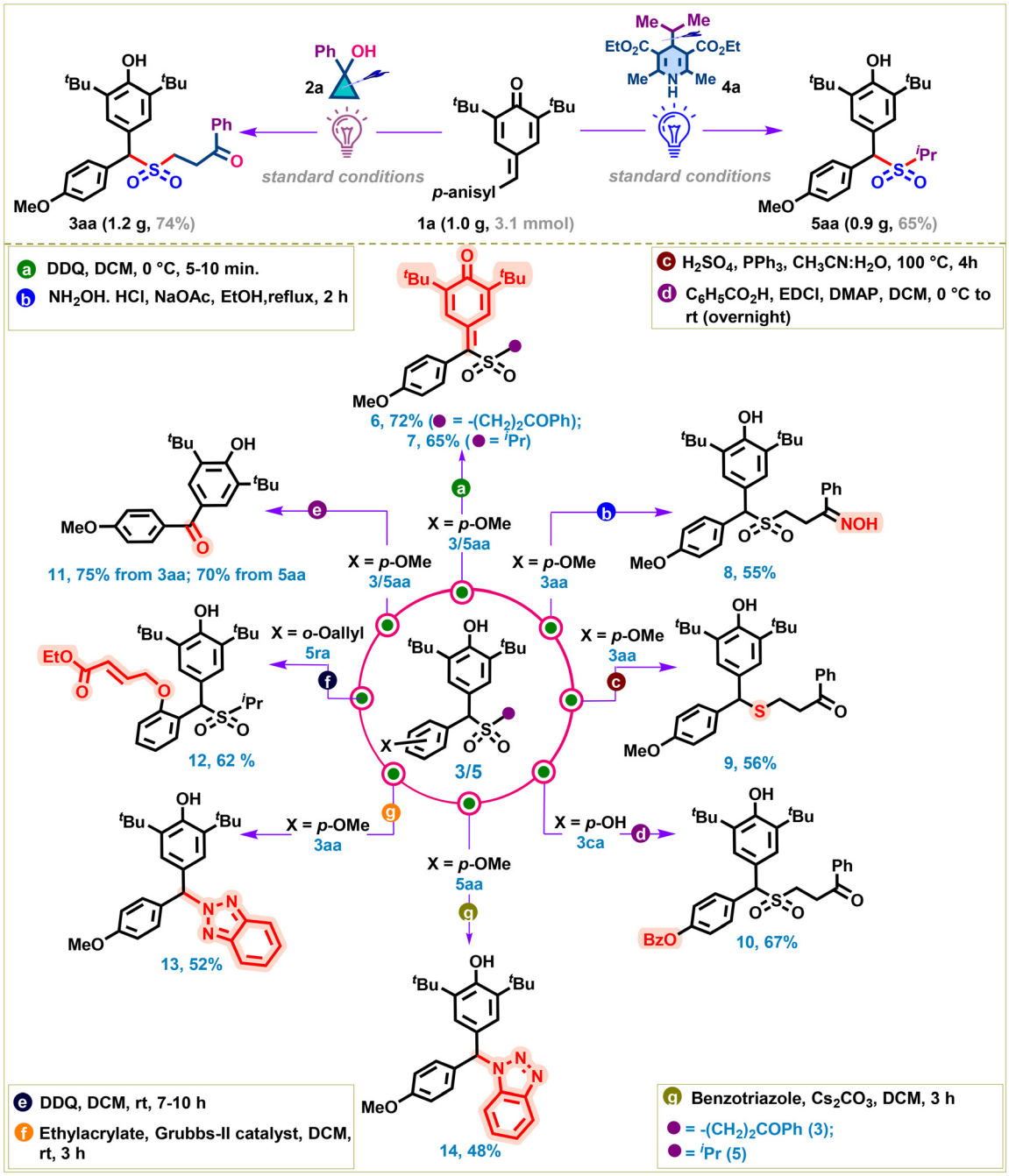


**Scheme 3** Gram-scale reaction and synthetic transformations on DAMS (**3**/**5**).

(**1**) with cyclopropanols (**2**) or 4-alkyl-1,4-DHPs (**4**), through a series of control experiments and spectroscopic studies shown in Fig. 3, employing **1a** and **2a**/**4a**. Firstly, to collect evidence for the radical nature of the reactions, we performed each of the couplings involving **1a** and **2a** in the presence of different trapping agents highlighted in Fig. 3A. The addition of radical trappers like TEMPO/diphenyl ethylene/BHT to each of the reactions, under the optimal conditions, resulted in either complete suppression or drastic reduction in the yields of the desired products **3aa**/**5aa** (Fig. 3A). Moreover, the TEMPO/diphenyl ethylene/BHT trapped adducts **15**–**18** (Fig. 3A) could be detected through HRMS (Fig. S1a–d, SI) in the case of the reaction involving **1a** and **2a** while the adducts **19**–**21** (Fig. 3A) could be HRMS-traced (Fig. S5a–d, SI) in the case of the reaction involving **1a** and **4a**. The light on–off experiments (Fig. 3B) conducted for each set of photoredox catalyzed reactions involving **1a** and **2a** or **4a** indicate that the **3aa**/**5aa** formation depends on constant light irradiation under the optimized conditions and rules out the involvement of a radical chain reaction. From the Stern–Volmer quenching studies, in

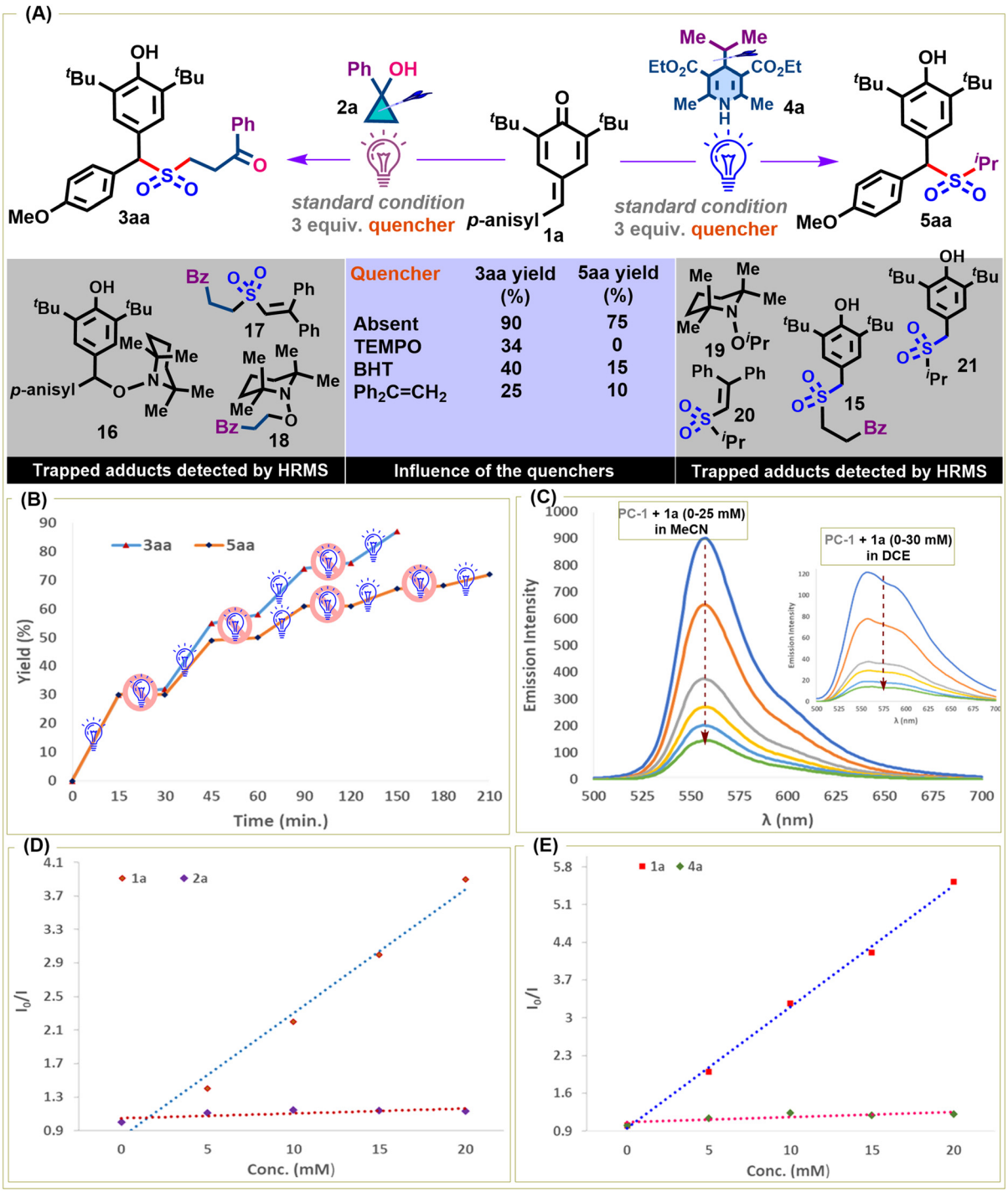


**Fig. 3** (A) Radical inhibition and trapping experiments. (B) Light on–off experiments. (C) Fluorescence quenching spectrum of **PC-1′** on incremental addition of **1a** (0–25 mM in MeCN; 0–30 mM in DCE). (D) Stern–Volmer quenching plot of **PC-1** against varying concentrations of **1a** and **2a**. (E) Stern–Volmer quenching plot of **PC-1** against varying concentrations of **1a** and **4a**.

the context of reactions involving **1a** and **2a**/**4a**, it was found that there was no significant effect of **2a**/**4a** on the emission profile of the excited **PC-1**. On the other hand, the incremental addition of **1a** was found to exert a significant quenching effect on the emission intensity of **PC-1** (Fig. 3C–E), hinting at a SET event between *p*-QM and excited **PC-1**.

Based on the control experiments and detailed mechanistic studies and considering the related literature reports,[56] the plausible mechanisms underlying the two photoredox-catalyzed reactions developed in the present study are as shown in Scheme 4. First, in the context of the reaction of **1** and **2** involving $SO_2$-capture, a dual catalytic cycle is proposed. Both the

 

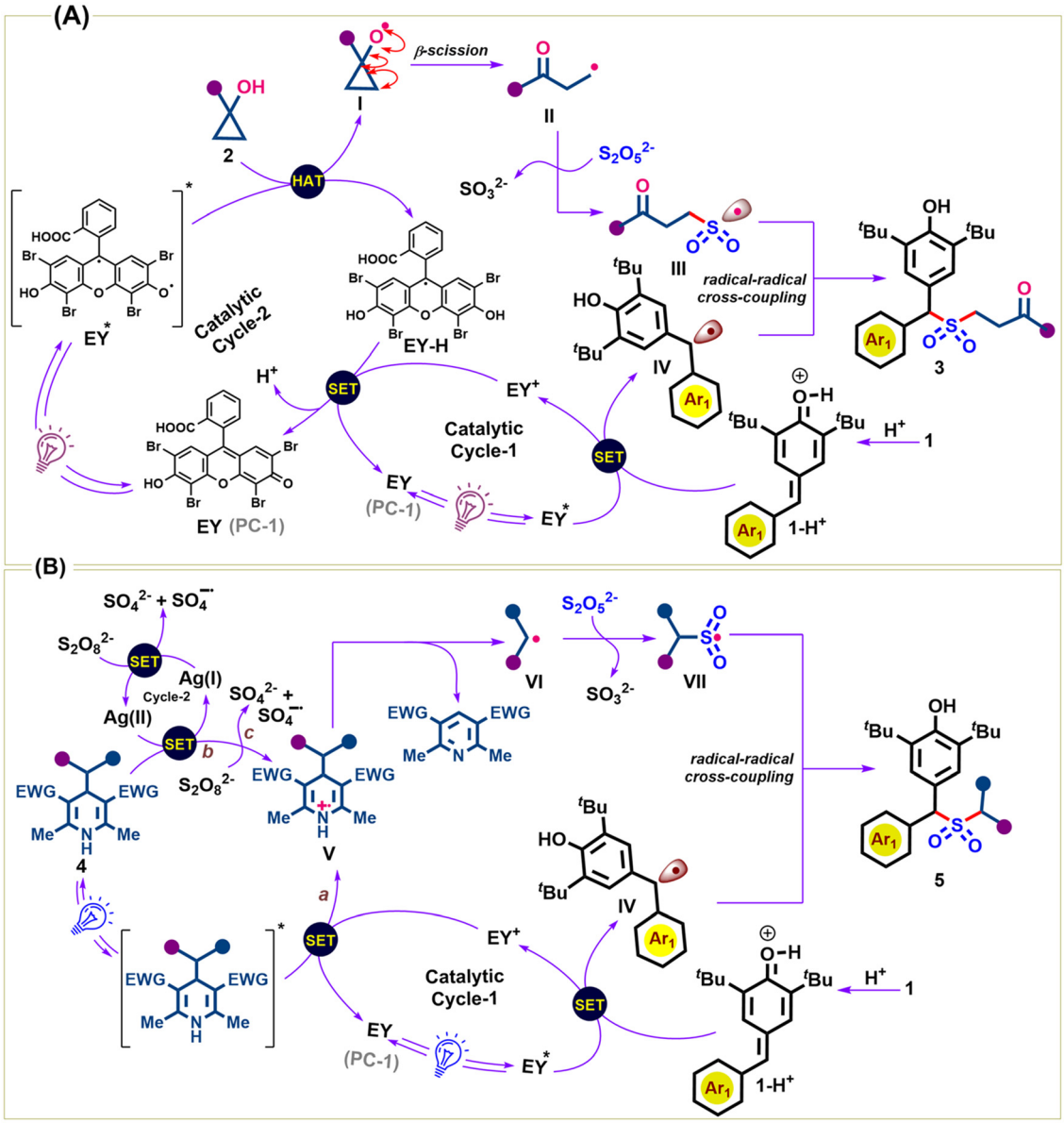


**Scheme 4** Plausible mechanisms for the synthesis of **3** and **5**.

outcome of the fluorescence quenching experiment and the redox potential data of cyclopropanols ($E_p$ = +1.06 − +1.54 V *vs.* SCE)[57] and the excited Eosin Y ($E_{1/2}$ (**EY***/EY$^{\cdot-}$) = +0.83 V *vs.* SCE)[58] ruled out the thermodynamic feasibility of any electron transfer between them. Therefore, mechanistically, the dual catalytic cycle is postulated to commence with the polarity-matched HAT between excited PC **EY*** and cyclopropanol **2** to generate the alkoxide **I** and EY-H. Subsequent strain-release driven ring scission in **I** produces the β-keto radical **II**, which on $SO_2$-capture generates the γ-keto sulfonyl radical **III**. On the other hand, the other catalytic cycle is postulated to involve the oxidative quenching of excited PC **EY*** with the proton-coupled *p*-QM **1** ($E_{1/2}$ (EY$^+$/**EY***) = −1.11 V *vs.* SCE)[58] and *p*-QM ($E_{red}$ = −0.20 V *vs.* SCE)[59–62] to generate the diarylmethyl radical **IV**. Then, the radical–radical cross-coupling between **III** and **IV** is presumed to be accountable for the formation of the γ-keto-alkylsulfonylated diarylmethane **3**. Lastly, the reverse HAT (RHAT) or reduction of the oxidised PC EY$^+$ by EY-H regenerates the photocatalyst EY, thereby closing both the catalytic cycles. Similar to the observation by Wu *et al.*,[63] the enhancement in the HAT-capability of PC EY in the presence of a Brønsted acid, besides facilitating the reductive SET on **IV**, is proposed to account for the dramatic improvement in the reaction efficiency in the presence of TFA.

Similarly, the access to **5** through the reaction of **1** and **4** *via* $SO_2$-capture in the presence of TFA is mechanistically postulated, as shown in Scheme 4B. The photoredox cycle commences with the oxidative quenching of excited PC **EY*** with the proton-coupled *p*-QM **1**, ($E_{1/2}$ (EY$^+$/**EY***) = −1.11 V *vs.* SCE)[58] and *p*-QM ($E_{red}$ = −0.20 V *vs.* SCE)[59–62] to generate the diaryl-

methyl radical **IV** and oxidized PC $EY^+$. The formation of the other coupling partner is postulated to be derived through pathways **a**, **b**, and **c**, highlighted in Scheme 4B. Through path **a**, the oxidative SET from the photoexcited 4-alkyl-1,4-DHP ($E^*_{red} = -1.90 - -2.28$ V *vs.* SCE)[64] to the oxidized $EY^+$ ($E_{1/2}(EY^+/EY)$ = +0.78 V *vs.* SCE)[58] is believed to close the photoredox cycle while facilitating the generation of intermediate **V** and subsequently the alkyl radical **VI** *via* aromaticity driven C-4 bond scission. Simultaneously, the formation of **V** and subsequently **VI** is also postulated through the oxidation of 4-alkyl-1,4-DHP by Ag(I)/Ag(II)-catalysis in the presence of persulfate, as well as directly by persulfate, which constitutes paths **b** and **c**, respectively. Subsequent $SO_2$-capture by the alkyl radical **VI** gives rise to the alkylsulfonyl radical **VII** for radical–radical cross-coupling with **IV** to furnish **5** eventually.

## Computational studies

To further strengthen our proposed mechanism, we explored the proposed pathways through density functional theory (DFT) studies at the SMD/PBE0(D3BJ)/def2tzvp//PBE0(D3BJ)/def2svp level of theory. For this, **1b** was employed as the model *p*-QM, while **2a** and **4a** were used as the model cyclopropanol and 4-alkyl-1,4-DHP partner, respectively. The free energy profile diagram, along with the ChemDraw structures and DFT-optimized geometries of different intermediates and transition states, is depicted in Fig. 4.

For the first reaction comprising a dual catalytic cycle, catalytic cycle-1 involves the reaction of excited PC **EY*** with protonated *p*-QM (**1b**-$H^+$) to form **IV** and $\mathbf{EY}^{+\bullet}$. Here, **EY*** oxidizes to $\mathbf{EY}^{+\bullet}$, and **1b**-$H^+$ reduces to **IV**. The free energy of this reaction is calculated to be −3.3 kcal $mol^{-1}$, and the C–O bond length changes from 1.316 Å in **1b**-$H^+$ to 1.355 Å in **IV**. Catalytic cycle-2 involves 1-phenyl-1-hydroxycyclopropane **2a**, which undergoes a HAT reaction with excited PC $\mathbf{EY}^*$ to form the alkoxide radical **I** and $[\mathbf{EY\text{-}H}]^\bullet$. The reaction is found to be exergonic with $\Delta G$ = −8.1 kcal $mol^{-1}$ and hence feasible under the reaction conditions. It is important to note that in our recent work[46] $DABCO^{+\bullet}$ facilitated the HAT from cyclopropanol, where the reaction was found to be slightly endergonic by $\Delta G$ =

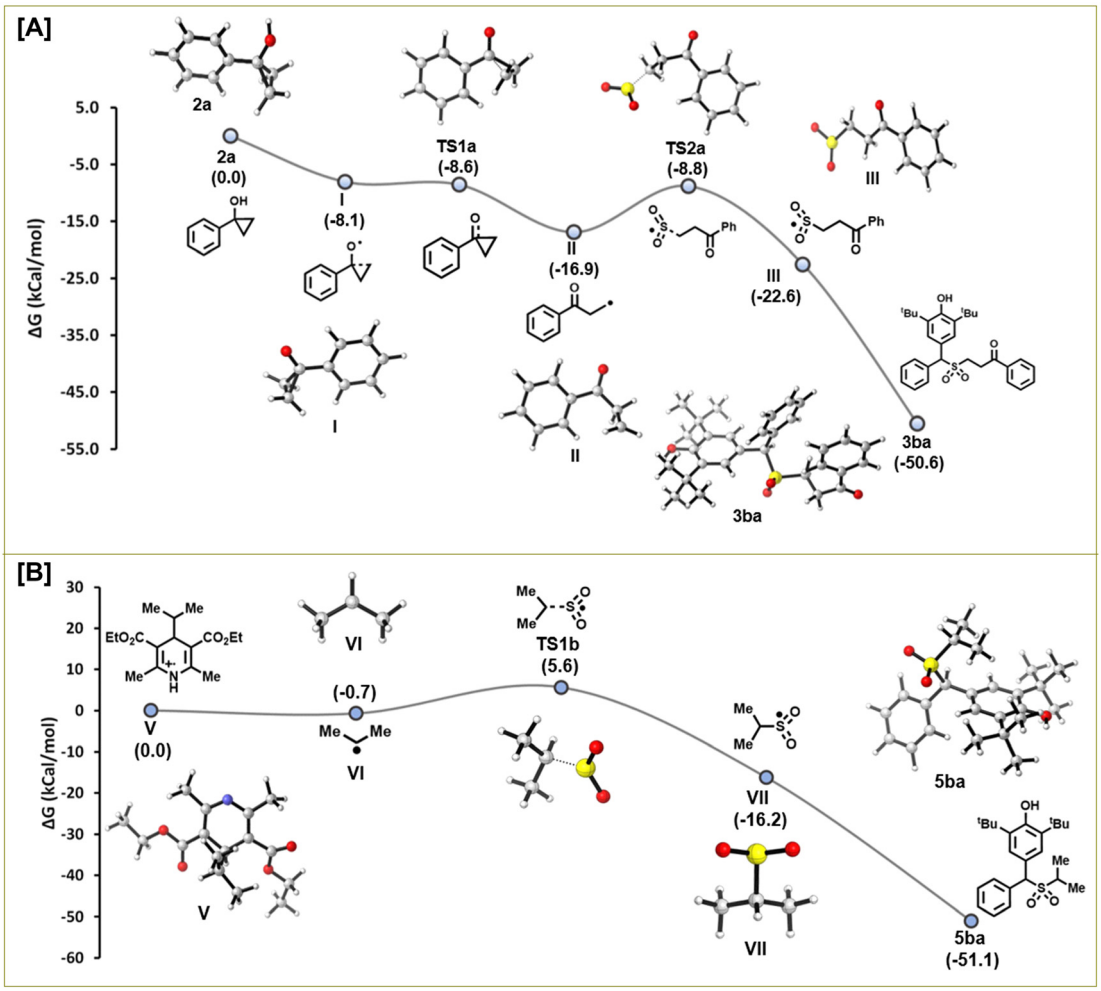


**Fig. 4** Free energy profiles for the proposed mechanisms (A) and (B) at the SMD/PBE0(D3BJ)/def2tzvp//PBE0(D3BJ)/def2svp level of theory.

4.7 kcal mol$^{-1}$. Hence, **EY*** works better as an oxidizing agent than DABCO (1,4-diazabicyclo[2.2.2]octane).

**I** is an oxygen-centred radical species, and the C–O bond length is found to decrease from 1.390 to 1.280 Å, clearly indicating the development of C–O double bond character. Then, the oxygen-centered radical species **I** is converted to the carbon-centered radical **II** through β-scission, *via* transition state **TS1a**. At **TS1a**, the C–O bond length further decreases to 1.249 Å, whereas the breaking C–C bond increases from 1.587 to 1.803 Å, implying a product-like transition state. The activation barrier for this step is −0.5 kcal mol$^{-1}$, implying the feasibility of the step. The carbon-centered radical **II** thus formed captures $SO_2$ to form the γ-keto sulfonyl radical **III**, and the reaction is spontaneous as $\Delta G$ = −13.8 kcal mol$^{-1}$. Then, radical **III** couples with **IV** to form the final product **3ba**. This radical coupling is found to be highly exergonic with $\Delta G$ = −41.8 kcal mol$^{-1}$, implying the spontaneity of the process for the synthesis of γ-keto alkylsulfonylated diarylmethanes. Lastly, the spontaneity of the reverse HAT (RHAT) between [**EY-H**]$^{\bullet}$ and **EY**$^{+}$ or reduction of the oxidised PC **EY**$^{+}$ by [**EY-H**]$^{\bullet}$ to regenerate the PC **EY** and thereby close both the catalytic cycles is supported by the free energy change of −36.9 kcal mol$^{-1}$.

Similarly, in the context of the reaction between **1b** and **4a** (Fig. 4B), the radical cation **V** generated through pathways **a**, **b**, and **c** depicted in Scheme 4 facilitates the formation of the isopropyl radical (**VI**) *via* the aromaticity-driven $C_4$-bond scission in **V**. This step is feasible as $\Delta G$ for the process is found to be −0.7 kcal mol$^{-1}$. Subsequent capture of $SO_2$ by **VI** furnishes the sulfur-centered radical **VII**. The reaction proceeds with the formation of transition state **TS1b** with an activation barrier of 6.3 kcal mol$^{-1}$, and the C–S bond length is 1.838 Å. Next, the isopropyl sulfonyl radical **VII** reacts with the diarylmethyl radical **IV** (formed similarly to that described *vide supra* for the first mechanism) to furnish the final product **5ba**. The reaction is spontaneous with $\Delta G$ = −34.9 kcal mol$^{-1}$ and favours the synthesis of alkylsulfonylated diarylmethanes.

## Biological studies

Taking into account the well-documented therapeutic potential of the DAMS scaffold as well as the γ-ketosulfone motif,[7,9,10] we were motivated to assess the anticancer activity of some selected compounds (entries 1–20, Table 1) against the oral squamous cell carcinomas (OSCC cell lines) **H357** and **SCC9**. The cell viability of these compounds on the OSCC cell lines **H357** and **SCC9** was determined by MTT assay. All the compounds were screened at 0.5, 2.5, 5, and 10 μM concentrations. Furthermore, we calculated the $IC_{50}$ (concentration for 50% of the cell death) values of the compounds, which are highlighted in Table 1, from the slope of the cell viability (%) *vs.* drug concentration (μM) plots in each cell line for each compound. All the tested compounds, except compound **3ao**, exhibited greater than 50% reduction in cell viability within 10 μM in both cell lines. Among them, four compounds **3ga**, **5ha**, **5ia**, and **5oa** had $IC_{50} \leq 5$ μM in both **H357** and **SCC9** (entries 1, 15, 16 and 18, Table 1). The plots of cell viability

**Table 1** $IC_{50}$ values of 20 compounds in the **H357** and **SCC9** cell lines

| S. no. | Compounds | $IC_{50}$ values (in μM) | |
|---|---|---|---|
| | | **H357** | **SCC9** |
| **1** | **3ga** | **4.91** | **4.90** |
| 2 | **3ia** | 6.25 | 5.01 |
| 3 | **3na** | 5.22 | 5.62 |
| 4 | **3ta** | 6.54 | 7.92 |
| 5 | **3ea** | 5.51 | 5.24 |
| 6 | **3xa** | 6.68 | 5.96 |
| 7 | **3pa** | 5.33 | 5.33 |
| 8 | **3oa** | 6.02 | 5.61 |
| 9 | **3wa** | 7.32 | 5.33 |
| 10 | **3an** | 8.83 | 5.19 |
| 11 | **3ao** | 10.37 | 5.67 |
| 12 | **3ap** | 8.27 | 5.47 |
| 13 | **5fa** | 7.09 | 5.87 |
| 14 | **5ga** | 8.40 | 8.44 |
| **15** | **5ha** | **4.74** | **3.71** |
| **16** | **5ia** | **5.00** | **4.37** |
| 17 | **5pa** | 5.32 | 5.29 |
| **18** | **5oa** | **4.02** | **4.41** |
| 19 | **5xa** | 8.13 | 6.96 |
| 20 | **5ta** | 5.19 | 5.18 |

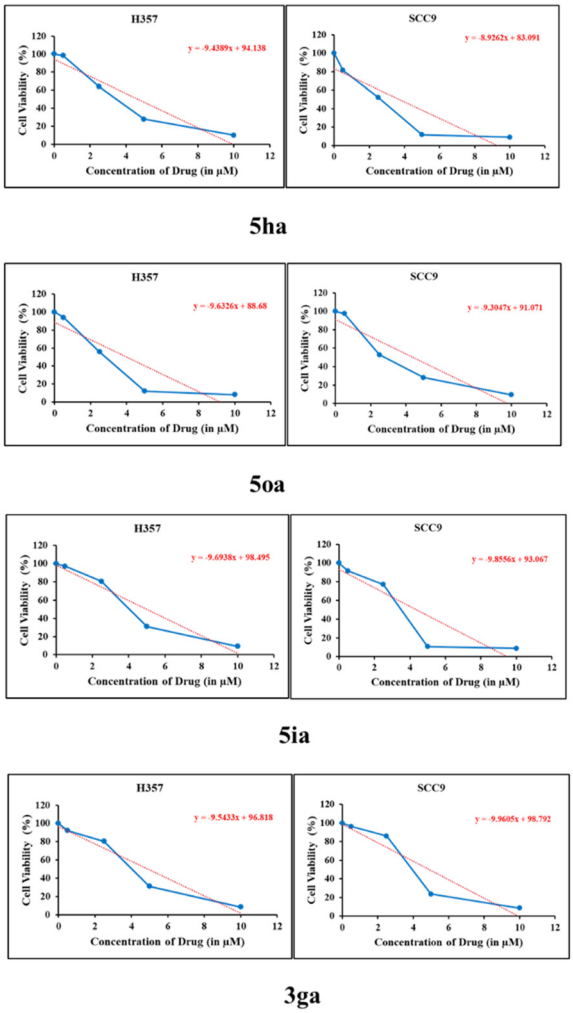


**Fig. 5** Cell viability *versus* concentration of compounds.

*versus* concentration for those four compounds are shown in Fig. 5.

## Conclusions

In conclusion, a visible light photoredox catalyzed 1,6-hydrosulfonylation of *p*-QMs has been demonstrated for the efficient synthesis of γ-keto alkylsulfonylated and alkylsulfonylated diarylmethanes *via* the incorporation of sulfur dioxide as a key building block for the sulfonyl functionality. A broad substrate scope, mild reaction conditions, and easily accessible starting materials from feedstock chemicals constitute some of the key highlights of the approach. Some valuable synthetic transformations have been demonstrated on the accessed scaffolds. Control experiments and DFT studies were conducted to gain mechanistic insights. Also, pharmacological investigation of some of the representative compounds from our synthesized library revealed prominent anticancer activity against the tested oral cancer cell lines and provided leads for further investigation.

## Author contributions

Conceptualization: T. K. Synthetic studies: D. K. P., T. K. S. and R. K. Computational studies: S. G. P. Manuscript drafting through contribution from all the authors. The final version of the manuscript was approved by all the authors.

## Conflicts of interest

There are no conflicts to declare.

## Data availability

The data supporting this article have been included as part of the SI. Supplementary information: experimental details, characterization and analytical data. See DOI: **https://doi.org/10.1039/d5qo00981b**.

CCDC 2441977 contains the supplementary crystallographic data for this paper.[55]

## Acknowledgements

T. K. gratefully acknowledges the financial support from the Anusandhan National Research Foundation (ANRF), formerly the Science and Engineering Research Board (SERB), DST, India (CRG/2023/002467). Dr Rupesh Dash from ILS-Bhubaneswar is acknowledged for the bioactivity profiling. D. K. P. thanks the UGC, India, and T. K. S. and R. K. thank the Ministry of Education, India, for the SRFs. All the authors thank their respective institutes for the financial and infrastructural support.

## References

1 Á. Hernández, C. Rosales-Fernández, C. Miranda-Vera, A. Veselinova, P. G. Jambrina, P. García-García, P. A. García, D. Díez, M. Á. Castro and M. Fuentes, Insights into Podophyllotoxin Lactone Features: New Cyclolignans as Potential Dual Tubulin–topoisomerase II Inhibitors, *Arch. Pharm.*, 2025, **358**, e2400600.
2 J. L. Wu, N. Li, T. Hasegawa, J. I. Sakai, T. Mitsui, H. Ogura, T. Kataoka, S. Oka, M. Kiuchi, A. Tomida, T. Turuo, M. Li, W. Tang and M. Ando, Bioactive Secolignans from Peperomia Dindygulensis, *J. Nat. Prod.*, 2006, **69**, 790–794.
3 S. Shen, Y. Tong, Y. Luo, L. Huang and W. Gao, Biosynthesis, Total Synthesis, and Pharmacological Activities of Aryltetralin-Type Lignan Podophyllotoxin and Its Derivatives, *Nat. Prod. Rep.*, 2022, **39**, 1856–1875.
4 G. L. Zhang, N. Li, Y. H. Wang, Y. T. Zheng, Z. Zhang and M. W. Wang, Bioactive Lignans from Peperomia Heyneana, *J. Nat. Prod.*, 2007, **70**, 662–664.
5 A. Pagliara, B. Testa, P.-A. Carrupt, P. Jolliet, C. Morin, D. Morin, S. S. Urien, J.-P. Tillement and J.-P. Rihoux, *Molecular Properties and Pharmacokinetic Behavior of Cetirizine, a Zwitterionic H 1-Receptor Antagonist, Molecular Properties and Pharmacokinetic Behavior of Cetirizine, a Zwitterionic H 1-Receptor Antagonist*, 1998.
6 U. Gulati, R. Gandhi and J. K. Laha, Benzylic Methylene Functionalizations of Diarylmethanes, *Chem. – Asian J.*, 2020, **15**, 3135–3161.
7 Z.-Q. Liu, P.-S. You, L.-D. Zhang, D.-Q. Liu, S.-S. Liu and X.-Y. Guan, TBAB-Catalyzed 1,6-Conjugate Sulfonylation of Para-Quinone Methides: A Highly Efficient Approach to Unsymmetrical Gem-Diarylmethyl Sulfones in Water, *Molecules*, 2020, **25**, 539.
8 P. Devendar and G.-F. Yang, Sulfur-Containing Agrochemicals, *Top. Curr. Chem.*, 2017, **375**, 82–82.
9 G. Yu, S. Chen, S. Guo, B. Xu and J. Wu, Trifluoromethylpyridine 1,3,4-Oxadiazole Derivatives: Emerging Scaffolds as Bacterial Agents, *ACS Omega*, 2021, **6**, 31093–31098.
10 H. F. Piedra, I. Tagarro and M. Plaza, EDA Complex Photochemistry as a Strategy for C–S Bond Formation, *Org. Chem. Front.*, 2025, **12**, 3920–3941.
11 A. Action, *"Sulfones—Advances in Research and Application: 2013 Edition: Scholarly Brief." Sulfones—Advances in Research and Application: 2013 Edition: Scholarly Brief*, Scholarly Editions, Atlanta, USA, 2013.
12 S. Patai, Z. Rappoport and C. Stirling, *The Chemistry of Sulphones and Sulphoxides*, Wiley, 1988.
13 A. El-Awa, M. N. Noshi, X. M. du Jourdin and P. L. Fuchs, Evolving Organic Synthesis Fostered by the Pluripotent Phenylsulfone Moiety, *Chem. Rev.*, 2009, **109**, 2315–2349.
14 B. M. Trost, Chemical Chameleons. Organosulfones as Synthetic Building Blocks, *Bull. Chem. Soc. Jpn.*, 1988, **61**, 107–124.
15 A. Hassner, E. Ghera, T. Yechezkel, V. Kleiman, T. Balasubramanian and D. Ostercamp, Stereoselective and

Enantioselective Synthesis of Five-Membered Rings via Conjugate Additions of Allylsulfone Carbanions, *Pure Appl. Chem.*, 2000, **72**, 1671–1683.

16 X. Cheng, S. Wang, Y. Wei, H. Wang and Y.-W. Lin, Metal-Free Hydrosulfonylation of α,β-Unsaturated Ketones: Synthesis and Application of γ-Keto Sulfones, *RSC Adv.*, 2022, **12**, 35649–35654.

17 X.-W. Feng, J. Wang, J. Zhang, J. Yang, N. Wang and X.-Q. Yu, Copper-Catalyzed Nitrogen Loss of Sulfonylhydrazones: A Reductive Strategy for the Synthesis of Sulfones from Carbonyl Compounds, *Org. Lett.*, 2010, **12**, 4408–4411.

18 G. Zhou, P. C. Ting and R. G. Aslanian, Palladium-Catalyzed Negishi α-Arylation of Alkylsulfones, *Tetrahedron Lett.*, 2010, **51**, 939–941.

19 J. Choi, P. Martín-Gago and G. C. Fu, Stereoconvergent Arylations and Alkenylations of Unactivated Alkyl Electrophiles: Catalytic Enantioselective Synthesis of Secondary Sulfonamides and Sulfones, *J. Am. Chem. Soc.*, 2014, **136**, 12161–12165.

20 T. Liu, J. Liu, S. Xia, J. Meng, X. Shen, X. Zhu, W. Chen, C. Sun and F. Cheng, Catalyst-Free 1,6-Conjugate Addition/Aromatization/Sulfonylation of Para-Quinone Methides: Facile Access to Diarylmethyl Sulfones, *ACS Omega*, 2018, **3**, 1409–1415.

21 X. Y. Guan, L. D. Zhang, P. S. You, S. S. Liu and Z. Q. Liu, 1,6-Conjugate Sulfonylation of Para-Quinone Methides: An Expedient Approach to Unsymmetrical Gem-Diarylmethyl Sulfones, *Tetrahedron Lett.*, 2019, **60**, 244–247.

22 P. Kumar, S. B. Kale, R. G. Gonnade and U. Das, Acid Mediated Sulfonylation of Para-Quinone Methides with Tosylmethyl Isocyanides for the Synthesis of Diarylmethyl Sulfones, *ChemistrySelect*, 2021, **6**, 7158–7161.

23 C. Qu, R. Huang, Y. Li, T. Liu, Y. Chen and G. Song, Selective Sulfonylation and Isonitrilation of Para-Quinone Methides Employing TosMIC as a Source of Sulfonyl Group or Isonitrile Group, *Beilstein J. Org. Chem.*, 2021, **17**, 2822–2831.

24 D. Gairola and R. K. Peddinti, Metal–Free Rapid Sulfonylation of Para –Quinone Methides and N –Arylmaleimides with Sulfonyl Hydrazides via a Free–Radical Pathway, *Asian J. Org. Chem.*, 2022, **11**, e202200517.

25 Y. T. Mei, H. Zhang, Y. Jiang, Y. J. Gu, J. L. Deng, D. Yang, L. H. Jing and M. S. Shi, Modular Access to Diarylmethyl Sulfonamides via Visible Light-Promoted Cross-Coupling Reactions, *Chem. Commun.*, 2024, **60**, 8589–8592.

26 M. Yang, H. Han, H. Jiang, S. Ye, X. Fan and J. Wu, Photoinduced Reaction of Potassium Alkyltrifluoroborates, Sulfur Dioxide and Para-Quinone Methides via Radical 1,6-Addition, *Chin. Chem. Lett.*, 2021, **32**, 3535–3538.

27 India Largest SO2 Emitter in the World, Says Greenpeace's New Analysis, India largest SO2 emitter in the World, says Greenpeace's new analysis," can be found under **https://www.greenpeace.org/india/en/press/4015/india-largest-so2-emitter-in-the-world-says-greenpeaces-new-analysis/**, 2021 (accessed: (05-06-2025)).

28 G. Liu, C. Fan and J. Wu, Fixation of Sulfur Dioxide into Small Molecules, *Org. Biomol. Chem.*, 2015, **13**, 1592–1599.

29 G. Qiu, K. Zhou, L. Gao and J. Wu, Insertion of Sulfur Dioxide via a Radical Process: An Efficient Route to Sulfonyl Compounds, *Org. Chem. Front.*, 2018, **5**, 691–705.

30 S. P. Blum, K. Hofman, G. Manolikakes and S. R. Waldvogel, Advances in Photochemical and Electrochemical Incorporation of Sulfur Dioxide for the Synthesis of Value-Added Compounds, *Chem. Commun.*, 2021, **57**, 8236–8249.

31 E. J. Emmett and M. C. Willis, The Development and Application of Sulfur Dioxide Surrogates in Synthetic Organic Chemistry, *Asian J. Org. Chem.*, 2015, **4**, 602–611.

32 A. K. Sahoo, A. Dahiya, A. Rakshit and B. K. Patel, The Renaissance of Alkali Metabisulfites as SO2 Surrogates, *SynOpen*, 2021, **5**, 232–251.

33 S. Ye, G. Qiu and J. Wu, Inorganic Sulfites as the Sulfur Dioxide Surrogates in Sulfonylation Reactions, *Chem. Commun.*, 2019, **55**, 1013–1019.

34 G. Chen and Z. Lian, Multicomponent Reactions Based on SO2 Surrogates: Recent Advances, *Eur. J. Org. Chem.*, 2023, e202300217.

35 Y. Meng, M. Wang and X. Jiang, Multicomponent Reductive Cross-Coupling of an Inorganic Sulfur Dioxide Surrogate: Straightforward Construction of Diversely Functionalized Sulfones, *Angew. Chem.*, 2020, **132**, 1362–1369.

36 Y. Li, S. Chen, M. Wang and X. Jiang, Sodium Dithionite-Mediated Decarboxylative Sulfonylation: Facile Access to Tertiary Sulfones, *Angew. Chem., Int. Ed.*, 2020, **59**, 8907–8911.

37 J. M. R. Narayanam and C. R. J. Stephenson, Visible Light Photoredox Catalysis: Applications in Organic Synthesis, *Chem. Soc. Rev.*, 2011, **40**, 102–113.

38 J. Xuan and W.-J. Xiao, Visible-Light Photoredox Catalysis, *Angew. Chem., Int. Ed.*, 2012, **51**, 6828–6838.

39 M. Reckenthäler and A. G. Griesbeck, Photoredox Catalysis for Organic Syntheses, *Adv. Synth. Catal.*, 2013, **355**, 2727–2744.

40 C. K. Prier, D. A. Rankic and D. W. C. MacMillan, Visible Light Photoredox Catalysis with Transition Metal Complexes: Applications in Organic Synthesis, *Chem. Rev.*, 2013, **113**, 5322–5363.

41 K. L. Skubi, T. R. Blum and T. P. Yoon, Dual Catalysis Strategies in Photochemical Synthesis, *Chem. Rev.*, 2016, **116**, 10035–10074.

42 N. A. Romero and D. A. Nicewicz, Organic Photoredox Catalysis, *Chem. Rev.*, 2016, **116**, 10075–10166.

43 M. H. Shaw, J. Twilton and D. W. C. MacMillan, Photoredox Catalysis in Organic Chemistry, *J. Org. Chem.*, 2016, **81**, 6898–6926.

44 T. K. Sahu, A. Vishwakarma, V. Kumar, R. Khan and T. Khan, Thermal vs. Visible-Light Photoredox-Catalyzed Cascade Radical Cyclization Involving SO2 Fixation to Access 6-Alkylsulfonylmethyl Phenanthridines, *Asian J. Org. Chem.*, 2024, **13**, e202400022.

45 R. Khan, D. K. Penthi, A. Chatterjee, C. Sahoo, S. G. Patra, V. A. Nagaraj and T. Khan, DABSO-Mediated Pummerer Reaction Enables One-Pot Synthesis of Pyrroloquinolines for Accessing Marinoquinolines: Mechanistic, Photophysical and Pharmacological Investigations, *Org. Chem. Front.*, 2025, **12**, 706–716.

46 A. Vishwakarma, T. K. Sahu, S. G. Patra, C. Paul and T. Khan, *Strain-Release-/Aromaticity-Driven Radical Generation and SO2-Capture Enables Acrylamides Bisfunctionalization via Photoredox Catalysis: Synthesis of S(VI) Functionalized Oxindoles*, 2025, DOI: **10.26434/chemrxiv-2025-npk7d**.

47 J. Sheng, J. Liu, L. Chen, L. Zhang, L. Zheng and X. Wei, Silver-Catalyzed Cascade Radical Cyclization of 2-(Allyloxy) Arylaldehydes with Cyclopropanols: Access to Chroman-4-One Derivatives, *Org. Chem. Front.*, 2019, **6**, 1471–1475.

48 L. Chang, Q. An, L. Duan, K. Feng and Z. Zuo, Alkoxy Radicals See the Light: New Paradigms of Photochemical Synthesis, *Chem. Rev.*, 2022, **122**, 2429–2486.

49 H. Yan, G. S. Smith and F.-E. Chen, Recent Advances Using Cyclopropanols and Cyclobutanols in Ring-Opening Asymmetric Synthesis, *Green Synth. Catal.*, 2022, **3**, 219–226.

50 G. Fumagalli, S. Stanton and J. F. Bower, Recent Methodologies That Exploit C–C Single-Bond Cleavage of Strained Ring Systems by Transition Metal Complexes, *Chem. Rev.*, 2017, **117**, 9404–9432.

51 A. Nikolaev and A. Orellana, Transition-Metal-Catalyzed C–C and C–X Bond-Forming Reactions Using Cyclopropanols, *Synthesis*, 2016, 1741–1768.

52 F. Wang, S. Yu and X. Li, Transition Metal-Catalysed Couplings between Arenes and Strained or Reactive Rings: Combination of C–H Activation and Ring Scission, *Chem. Soc. Rev.*, 2016, **45**, 6462–6477.

53 D. J. Mack and J. T. Njardarson, Recent Advances in the Metal-Catalyzed Ring Expansions of Three- and Four-Membered Rings, *ACS Catal.*, 2013, **3**, 272–286.

54 A. García-Domínguez, R. Mondal and C. Nevado, Dual Photoredox/Nickel-Catalyzed Three-Component Carbofunctionalization of Alkenes, *Angew. Chem., Int. Ed.*, 2019, **58**, 12286–12290.

55 Deposition numbers 2441977 for **5sa** contain the supplementary crystallographic data for this paper. D. K. Penthi, T.K. Sahu, R. Khan, S.G. Patra and T. Khan, CCDC 2441977: Experimental Crystal Structure Determination, 2025, DOI: **10.5517/ccdc.csd.cc2mz2g5**.

56 X.-Z. Fan, J.-W. Rong, H.-L. Wu, Q. Zhou, H.-P. Deng, J. D. Tan, C.-W. Xue, L.-Z. Wu, H.-R. Tao and J. Wu, Eosin Y as a Direct Hydrogen-Atom Transfer Photocatalyst for the Functionalization of C–H Bonds, *Angew. Chem., Int. Ed.*, 2018, **57**, 8514–8518.

57 A. Krech, V. Yakimchyk, T. Jarg, D. Kananovich and M. Ošeka, Ring-Opening Coupling Reaction of Cyclopropanols with Electrophilic Alkenes Enabled by Decatungstate as Photoredox Catalyst, *Adv. Synth. Catal.*, 2024, **366**, 91–100.

58 D. P. Hari and B. König, Synthetic Applications of Eosin Y in Photoredox Catalysis, *Chem. Commun.*, 2014, **50**, 6688–6699.

59 Q.-L. Wu, J. Guo, G.-B. Huang, A. S. C. Chan, J. Weng and G. Lu, Visible-Light-Promoted Radical Cross-Coupling of Para-Quinone Methides with N-Substituted Anilines: An Efficient Approach to 2,2-Diarylethylamines, *Org. Biomol. Chem.*, 2020, **18**, 860–864.

60 Rekha, S. Sharma and R. V. Anand, Visible-Light-Mediated Radical Reactions of Indoles with Para-Quinone Methides Using Eosin Y as an Organophotoredox Catalyst, *Org. Biomol. Chem.*, 2023, **21**, 6218–6224.

61 Q. Yang, G. Pan, J. Wei, W. Wang, Y. Tang and Y. Cai, Remarkable Activity of Potassium-Modified Carbon Nitride for Heterogeneous Photocatalytic Decarboxylative Alkyl/Acyl Radical Addition and Reductive Dimerization of Para-Quinone Methides, *ACS Sustainable Chem. Eng.*, 2021, **9**, 2367–2377.

62 J. Rostoll-Berenguer, V. García-García, G. Blay, J. R. Pedro and C. Vila, Organophotoredox 1,6-Addition of 3,4-Dihydroquinoxalin-2-Ones to Para-Quinone Methides Using Visible Light, *ACS Org. Inorg. Au*, 2023, **3**, 130–135.

63 H. Cao, D. Kong, L.-C. Yang, S. Chanmungkalakul, T. Liu, J.-L. Piper, Z. Peng, L. Gao, X. Liu, X. Hong and J. Wu, Brønsted acid-enhanced direct hydrogen atom transfer photocatalysis for selective functionalization of unactivated C (sp3)–H bonds, *Nat. Synth.*, 2022, **1**, 794–803.

64 G. S. Yedase, S. Venugopal, P. Arya and V. R. Yatham, Catalyst-Free Hantzsch Ester-Mediated Organic Transformations Driven by Visible Light, *Asian J. Org. Chem.*, 2022, **11**, e202200478.

 